

DEFORMATION INDEX APPLIED TO IMPACT

T. C. RANSOM,^{1,†} R. M. GAMACHE,² B. P. MASON,² H. D. LADOUCEUR,^{1,‡} C. M. ROLAND^{1,*}

¹NAVAL RESEARCH LABORATORY, CHEMISTRY DIVISION, CODE 6105, WASHINGTON, D.C. 20375-5342

²NAVAL POSTGRADUATE SCHOOL, DEPARTMENT OF PHYSICS, MONTEREY, CA 93943-5216

RUBBER CHEMISTRY AND TECHNOLOGY, Vol. 93, No. 2, pp. 261–273 (2020)

ABSTRACT

Almost three decades ago, S. Futamura devised the deformation index concept for determining the control parameter for the viscoelastic response of deformed elastomers. We have extended this concept to impact mitigation, wherein material hardness and energy dissipation typically both affect the behavior. Laboratory impact tests were carried out on a series of compounds to deduce the deformation index pertinent to the rubber component. We then analyzed ballistic experiments, wherein material failure is associated with more complex conditions. The utility and limitations of this approach are discussed. [doi:10.5254/rct.20.80362]

INTRODUCTION

Research and development efforts to understand collisions and ameliorate the damage from impact extend to a wide range of applications and technologies such as automotive collisions^{1,2} and with the proliferation of electric automobiles, to the crashworthiness of their batteries;^{3,4} collisions involving space debris,^{5,6} such as asteroids with the Earth;⁷ seismic activity;⁸ brain injuries due to head impact;^{9–12} and military helmets.^{13–17} The latter two problems are especially difficult to assess because of the complexity of the response of the brain (strain, negative and positive pressures, pressure gradients, rotation, and coup/contrecoup effects^{18–20}) to blast or ballistic assault.^{21–25} Collisions give rise to nonlinear deformations at high strain rates that may be accompanied by both physical (cavitation, phase transitions) and chemical changes.^{26–33}

The starting point in mitigating the effects of impact is understanding the factors underlying damage. Modeling and simulations of impact are widely developed, spanning molecular dynamic simulations,^{34,35} continuum mechanics,^{36–38} hydrocode, and finite element modeling.^{39–42} In this work we adopt a simple, intuitive approach based on the deformation index concept in which the interdependence among components is decoupled from the mechanical perturbation imposed on the system.⁴³ The objective is a predictive scheme that at least makes empirical test and evaluation procedures more efficient. The method has been applied to the rolling resistance of tires,⁴⁴ heat buildup in both pneumatic⁴⁴ and nonpneumatic tires,⁴⁵ and rubber fatigue.⁴⁶ In this method a property of the system is measured and correlated with the quantity E''/E^{*n} , where E'' is the dynamic loss modulus; E^* is the complex modulus, which for elastomers is nearly equivalent to the storage modulus; and n is the deformation index. This correlation follows from the equation⁴⁴

$$P = k_1 E'' / E^{*n} + k_2 \quad (1)$$

in which P is the property of interest and k_1 and k_2 are constants for a given system. The value of the index n yielding the best correlation of the measured P characterizes the nature of the deformation. Strain, energy, and stress controls correspond to $n=0$, 1, and 2, respectively, although nonintegral values are possible for more convoluted processes.

[†]Current address: Naval Surface Warfare Center–Indian Head, Indian Head, MD 20640

[‡]Deceased November 27, 2019

*Corresponding author. Email: croland52@gmail.com

We use the deformation index to analyze impact data via both laboratory experiments and ballistic tests. The objective is to assess the nature of the deformation experienced by the rubber component to identify the properties of elastomer coatings underlying the protection afforded to armor systems subjected to impact. This topic has been explored in many previous studies,^{47–50} motivated by the fact that energy dissipation and hardness both contribute to impact protection generally^{51–54} and for armor using elastomer coatings.^{49,55}

EXPERIMENTAL

The polymers herein were random copolymers of acrylonitrile and butadiene, NBR (Nipol, Zeon Chemical, Louisville, KY, USA), or styrene and butadiene, SBR (Duradene, Firestone Polymers, Akron, OH, USA or emulsion SBR, Lion Elastomers, Port Neches, TX, USA). Curing was effected using sulfur, 2-2'-dithiobis(benzothiazole), zinc oxide, and stearic acid. For the deformation index analysis to be applicable, the ratio of the storage and loss moduli cannot be constant, and the accuracy increases for greater variation of the elastic and viscous properties of the tested compounds. For this reason the dynamic moduli were varied in two ways, by incorporating reinforcing carbon black (N110 or N990) and by using polymers with different glass transition temperatures (T_g). The latter is relevant when T_g is close to the test temperature and for high strain rate experiments. The compounds are listed in Tables I–IV.

Isothermal dynamic mechanical measurements at various temperatures were carried out on a Q800 dynamic mechanical analyzer (TA Instruments, Newcastle, DE, USA) in tension mode, over the frequency range $0.063 \leq \omega$ (rad/s) ≤ 200 at a strain amplitude equal to 0.1%. Time–temperature shift factors were determined from master curves of the loss tangent, with small vertical shifts applied to superpose the storage and loss moduli⁵⁶ and obtain the viscoelastic response at higher frequencies.

For the rebound experiment, 2.5 cm diameter, 1 cm thick disks were placed on a steel base, with a cylindrical 28 g mass dropped from a fixed height of $h = 40$ cm. Five measurements of the rebound height were made, with the sample temperature of 50 °C to achieve sufficient resilience in all compounds. The glass fracture test was carried out on 75 mm \times 25 mm \times 0.1 mm optical glass, with 25 mm \times 50 mm \times 2 mm rubber coatings. The test temperature was also 50 °C. A 63 g, 25 mm diameter steel sphere was used as the projectile, released from varying heights by using a magnetic release. The drop height was increased incrementally until fracture was obtained. The test was repeated at this same height multiple times to ensure a minimum failure rate of at least 50%.

Ballistic tests at ambient temperature were carried out on a laminate of 5 mm thick rubber sheets attached to the front (strike-face) side of a 6 mm steel substrate (high hard steel; MIL-DTL-46100). The minimum velocity required for a 12.5 mm diameter steel projectile (MIL-DTL-46593B) to penetrate the laminate was determined, with complete penetration defined by perforation of a backside witness plate. The test conditions complied with MIL-STD-662, with a full description found elsewhere.⁵⁷

Finite element analysis (COMSOL Multiphysics®, Burlington, MA, USA) used a two-dimensional axisymmetric model of the rebound resiliometer test, with the dimensions and properties of the rubber target and steel drop weight chosen to match the experiment. The deformation index formalism uses frequency-dependent real and imaginary moduli; for the modeling the loss was taken as the viscosity via $E'' \tan \delta/3\omega$, where $\tan \delta$ is the loss tangent equal to the ratio of the loss and storage moduli. The extraction of the deformation index from the calculation followed the procedure in ref 46; to wit, the energy dissipated for each individual element was computed, the modulus increased 20%, and the model rerun to calculate the energy dissipated by that same element.

TABLE I
REBOUND TEST (at 50 °C)

$T_g, ^\circ\text{C}$	Filler	E' at 300 s ⁻¹ , MPa	E'' at 300 s ⁻¹ , MPa	Rebound, %
-20	0 ^a	3.2	0.47	61.8 ± 0.1
		3.4	0.45	61.8 ± 0.1
		3.5	0.52	64.2 ± 0.3
0	40 phr N990	6.1	0.90	58.2 ± 0.1
	20 phr N110	7.9	1.2	54.7 ± 0.3
	30 phr N110	15.5	2.5	48.6 ± 0.2
	40 phr N110	23.7	4.0	44.3 ± 0.05
	0	5.3	2.2	30.3 ± 0.3
	40 phr N990	12.4	5.0	28.8 ± 1
	20 phr N110	18.3	7.1	24.6 ± 0.1
0	0	34.7	12.2	22.0 ± 0.1
		52.9	16.6	20.8 ± 0.8

^a Varying crosslink density.

RESULTS AND DISCUSSION

REBOUND TESTS

As an initial experiment, resilience determinations were carried out for a steel projectile falling from a fixed height onto a rubber disc; a test temperature of 50 °C was chosen to give measurable rebound heights for all compounds (Table I). Such drop tests are commonly used to characterize the dynamic behavior of materials; the square root of the rebound height relative to the drop height is known as the coefficient of restitution.⁵⁸ For these tests we calculated the Pearson linear correlation coefficient for Eq. 1, with P being the measured rebound of the projectile, by using deformation indices in the range $0 \leq n \leq 2$. As shown in Figures 1 and 2a, the correlation of the experimental rebound data with E''/E^{*n} was greatest for $n=0.7$ ($R=98\%$). Note the analysis requires taking into account the rate dependence of the dynamic properties. From video of the impact, we estimated the strain rate to be approximately 300 s⁻¹, a value that is consistent with the ratio of the impact speed

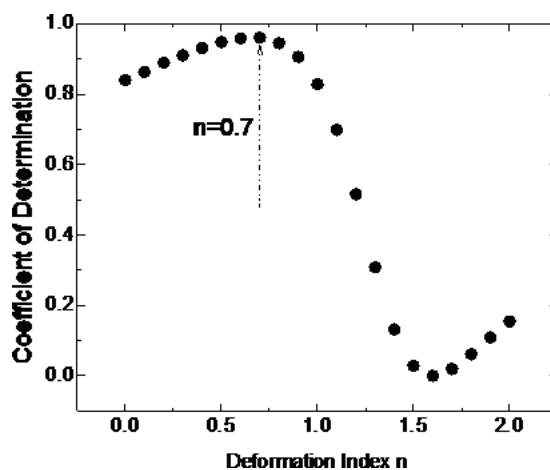


FIG. 1. — Goodness-of-fit of E''/E^{*n} for rebound data, with the best correlation achieved for $n=0.7$.

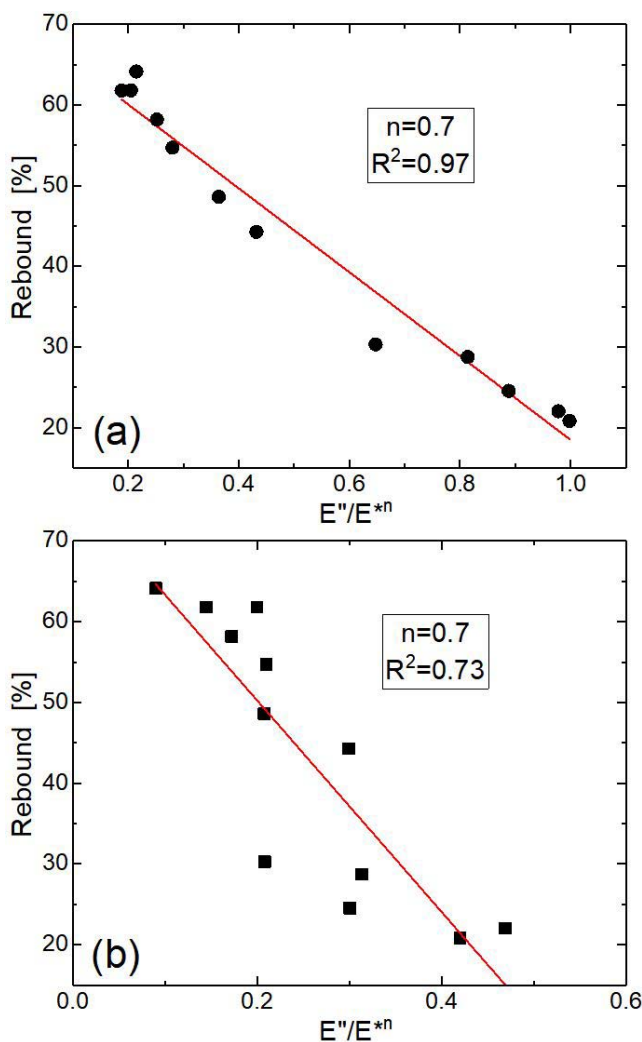


FIG. 2. — Rebound measured for the coatings in Table I vs the deformation index variable with $n = 0.7$ and dynamic properties at (a) 300 s^{-1} and (b) 0.1 s^{-1} . Coefficient of determination is indicated.

($\sqrt{2gh}$; $g = 9.8 \text{ m/s}^2$) to rubber thickness (280 s^{-1}). As shown in Figure 2b, the correlation of the rebound data with E''/E^{*n} deteriorates significantly if the dynamic moduli measured at 1 s^{-1} are used, rather than the appropriate values, obtained by time–temperature superposition, at 300 s^{-1} .

Our result, $n = 0.7$, is in agreement with the analysis of similar rebound experiments in ref 45. The question that arises is why dropping a weight from a constant height does not induce constant energy deformation ($n = 1$), corresponding to the gravitational potential in the absence of friction. To investigate this in more detail, we carried out finite element modeling of the rebound experiment. The deformation index was determined as a function of position in the rubber disk by computing the change in strain response of each element to a change in its stiffness. The results are displayed in Figure 3, where it can be seen that over most of the volume, $n = 1$; that is, constant energy deformation, consistent with a fixed drop height. However, in the vicinity of the impact n varies strongly with position. It is this complex interaction around the point of impact that causes the net

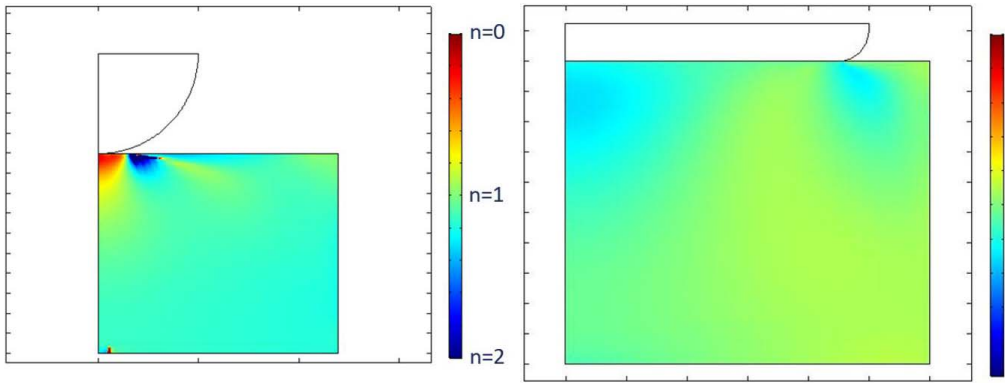


FIG. 3. — Finite element calculations of the deformation index as a function of position for (left) projectile tip similar to that used experimentally; (right) a flat projectile that more uniformly compresses the rubber disk. The scale bar spans the range of deformation indices from stress control ($n = 2$) to strain control ($n = 0$).

value of n to be less than unity. If the projectile cross-sectional area is significantly increased, close to that of the rubber disk, the latter now compresses uniformly (Figure 3). This alleviates the interactions at the point of impact, and the deformation index has a net value very close to unity.

Figure 4 shows the compression of the rubber as a function of time after impact. The calculation was carried out for two elastomers, with one elastomer having a 20% higher modulus. Interestingly, the compression of the cylinders is the same, independent of the rubber stiffness, up through roughly half the time before maximum penetration of the projectile. This “inertial” behavior is sensitive to the details of the finite element modeling, diminishing for a broader projectile or lower

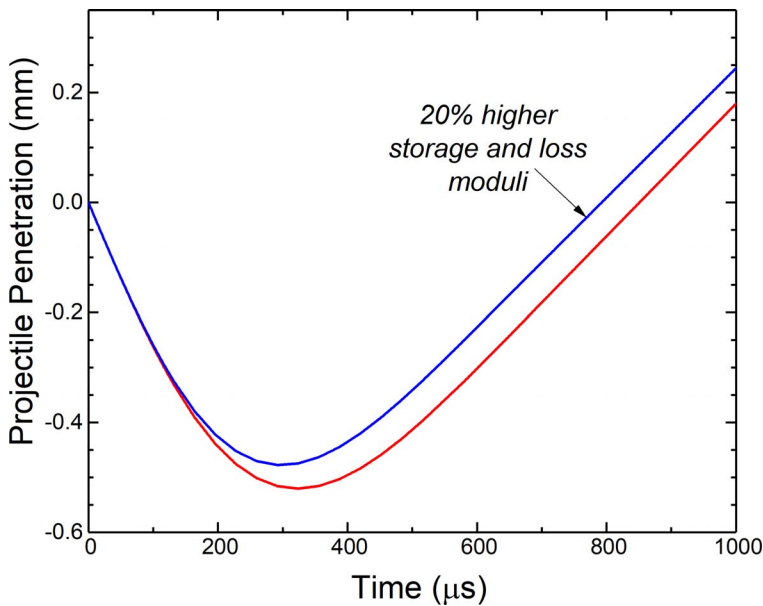


FIG. 4. — Finite element calculations of the penetration of the projectile for rubber disks having storage and loss moduli that differ by a factor of 1.2. Note the effect of rubber modulus becomes apparent only after the first 150 μs .

TABLE II
GLASS BREAKAGE TEST (at 50 °C)

T_g , °C	Filler	E' at $7.5 \times 10^3 \text{ s}^{-1}$, MPa	E'' at $7.5 \times 10^3 \text{ s}^{-1}$, MPa	Glass break height, cm	
-20	0 ^a	4.6	1.9	536 ± 50	
		4.4	2.2	536 ± 50	
		5.3	3.4	536 ± 50	
	40 phr N990	8.6	4.3	572 ± 50	
		20 phr N110	11	5.1	866 ± 100
		30 phr N110	24	19.1	866 ± 100
0	0	36	15.2	866 ± 100	
		14.3	16.2	899 ± 50	
		40 phr N990	32.2	34	932 ± 50
	40 phr N110	46.2	40	988 ± 50	
		30 phr N110	81	57	1,210 ± 75
		40 phr N110	106	62	1,210 ± 75

^a Varying crosslink density.

impact velocities. But at least initially the deformation is largely strain controlled, corresponding to $n=0$, and thus not dependent on the rubber properties. The significance of this becomes apparent in the glass fracture tests.

GLASS FRACTURE TESTS

To extend the deformation index method to failure, a glass/elastomer laminate was used as the target, with the drop height varied to determine the minimum necessary to fracture the (backside) glass. The compounds for this test are listed in Table II, along with their dynamic moduli. Rate effects are important even for rigid solids,⁵⁹ with frequency dependence herein obtained (using time–temperature superpositioning) at the frequency corresponding to the measured strain rate of $7.5 \pm 1.5 \text{ s}^{-1}$. The error bars on this strain rate reflect the different drop heights required to break the glass for different coating, which of course changes the impact velocity and thus the strain rate. Figure 5 shows a plot of the minimum height to break the glass as a function of E''/E'^n (Eq. 1, with P the drop height). The scatter in the data is larger than for the rebound tests, as expected for failure properties. The best correlation is for $n=0.35 \pm 0.1$. This signifies substantial strain control of the fracture process, in accord with the results in Figure 4, showing that compression of the elastomer during the impingement phase is initially independent of the rubber modulus. The consequent flexure of the glass governs its fracture, which likely occurs before bottoming out and subsequent rebound of the projectile.

BALLISTIC TESTS

We extended the failure experiments to ballistic tests. A powder gun was used to propel a steel projectile at normal incidence to a rubber-coated steel target, with measurement of the minimum velocity required for penetration of the bilayer (i.e., a 50% probability of complete penetration). The rubber compounds, listed in Table III, were comprised of polymers having different T_g values, both with and without reinforcing filler. This variation ensured a range of values of the ratio of the loss and complex moduli. However, it is again necessary that the viscoelastic properties correspond to

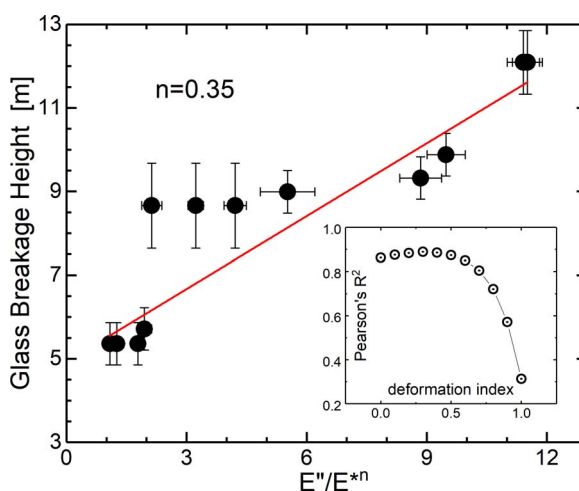


FIG. 5. — Minimum drop height to break glass having the rubber coatings in Table II vs the deformation index parameter with $n = 0.35$. Inset shows the fit quality as a function of n , with the maximum at $n = 0.35 \pm 0.1$.

the test frequency. For ballistic tests this is approximately 10^5 s^{-1} ,²⁸ requiring application of time–temperature superpositioning. Master curves of the dynamic moduli are shown in Figure 6, where it can be seen that ballistic impact causes the rubber response to encroach on the glass transition zone. This region of the viscoelastic spectrum is characterized by contributions from both the chain dynamics and local segmental motions. Because these have different time–temperature shift factors, time–temperature superpositioning breaks down in the transition zone.^{56,60} Thus, these master curves and the dynamic moduli obtained are only approximate.

The test results are displayed in Figure 7 in the form suggested by Eq. 1, with P the relative increase in the velocity of the projectile necessary to penetrate the laminate. The value of n yielding the strongest correlation is 1.3, although the scatter is substantial ($R^2 = 0.76$). The implication of $n = 1.3$ is that ballistic penetration is mainly energy driven, but with a significant stress-control component. Because reinforcing filler increases both the energy dissipation as well as the rubber stiffness, this suggests that the filled compounds should be superior to the gum coatings, an inference borne out by the data (Figure 8). Of course, this conclusion does not require the

TABLE III
BALLISTIC TEST ($n = 1.3$)

Sample	$T_g, ^\circ\text{C}$	N110 filler, phr	E' at 10^5 s^{-1} , MPa	E'' at 10^5 s^{-1} , MPa	E''/E^*n	Increase in penetration velocity, %
SBR-1g	-27	0	48	77	0.219	40.9
SBR-1f		40	155	138	0.134	42.2
SBR-2g	-42	0	22	27.4	0.268	46.4
SBR-2f		40	105	73	0.133	45.2
SBR-3g	-55	0	10.6	11.3	0.321	38.6
SBR-3f		40	69.	44.	0.143	46.4
SBR-4g	-70	0	4.9	2.1	0.238	40.1
SBR-4f		40	52.	15.	0.084	47.5

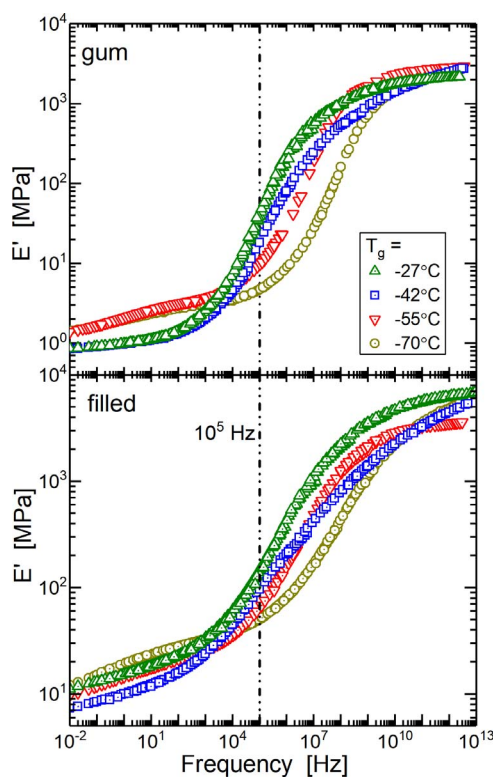


FIG. 6. — Dynamic mechanical master curves at a reference temperature of 25 °C for the elastomers in Table III: (top) unfilled; (bottom) carbon black reinforced. The horizontal dotted line denotes the approximate frequency of the ballistic test. With increasing T_g of the coating, the impact occurs further into the glass transition zone.

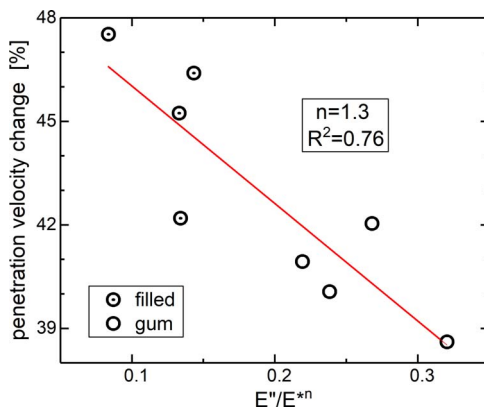


FIG. 7. — Relative increase in the minimum projectile velocity for complete penetration of the rubber/steel laminate for the compounds listed in Table III. Deformation index best describing the data, $n = 1.3$, has a Pearson's correlation coefficient of 87%.

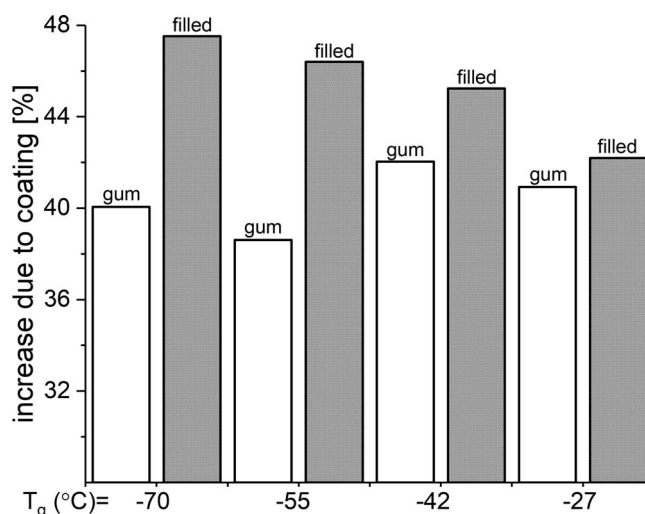


FIG. 8. — Comparison of the relative increase in penetration velocity for targets having coatings with and without reinforcing carbon black.

deformation index analysis, because it is evident directly from the test results. However, the purpose of this study was to assess a potential method of circumventing, or at least making more efficient, a “make-and-break” empirical approach to developing better rubber ballistic coatings.

The interpretation of the data in Figure 7 is complicated because the high strain rates associated with ballistic impact are proximate to the rubber-to-glass transition.^{28,34} Such a viscoelastic phase change is unaccounted for by the deformation index analysis as carried out herein. The onset of this phase change is evident in images of the rubber coatings after penetration (Figure 9a,b). Lower T_g compounds exhibit extensive tearing, a rubbery-like response, whereas the high T_g coatings fail in a more brittle manner, with the hole produced in the rubber about the same size as the projectile. These contrasting behaviors are typical of the modes of failure of rubber coatings subjected to ballistic impact.^{27,55} Note that the presence of reinforcing filler yields a response more like that of the higher T_g compounds (Figure 9c,d), which presumably contributes to their better performance.

An analysis using the deformation index has merit only if it is predictive. To assess this, we examined two polymers, polyvinylethylene and polyurea, previously found to have equivalent ballistic performance when used as coatings over steel.⁵⁵ This equivalence implies that the quantity E''/E^{*n} will be the same, using $n = 1.3$ as determined above. (For this analysis we used shear moduli, because the rubbers were uncured.) These two materials have substantially different storage and loss moduli (Table IV), providing a stern test of the method. The deformation index quantity $G''/G^{*1.3}$ is equivalent within a few percent for the rubbers, consistent with their same ballistic performance.

DISCUSSION

There are three main assumptions inherent to applying the deformation index analysis to impact or ballistic experiments, and they are described below.

- (i) The effects of strain and time are decoupled, allowing their separation. This enables application of a superposition integral to calculate the stress⁵⁶

viscoelastic properties relies on dynamic mechanical characterization that is then used to interpret the transient impact response. This assumption has been tested for various elastomers, with the conclusion that it is valid except near the glass transition zone.⁶²

- (iii) As mentioned, to obtain the viscoelastic moduli at the impact strain rates required invoking the time–temperature superposition principle, which is known to fail for polymers in the glass transition zone.^{56,60}

Because the strain rates for the rebound and glass breakage tests were not high ($<10^4 \text{ s}^{-1}$), the complexities of the glass transition (assumptions ii and iii) are not especially pertinent for these experiments. For this reason, the deformation index analysis yields a reliable description of the behavior of the rubbers in these tests. For the ballistic experiments herein, the encroachment into the glass transition zone (Figure 6) introduces substantial error. Nevertheless, the value of the deformation index obtained for ballistic tests of the compounds in Table III was able to predict with surprising accuracy the ballistic performance of the two polymers in Table IV. Obviously, more general application of the method to impact tests should use direct characterization of the viscoelastic properties at the relevant strain rates.

CONCLUSIONS

The results reported herein demonstrate the utility of the deformation index analysis. It describes simple rebound/resilience experiments, including effects due to the complex interactions at the sample interface. When applied to glass fracture, the analysis correctly accounts for the behavior during the initial compression, distinct from full penetration and recoil. And notwithstanding complications from the rubber-to-glass transition in ballistic tests, which introduces inaccuracies into the use of time–temperature superpositioning to obtain the viscoelastic properties of the rubber at the relevant strain rates, the deformation index approach was applicable to ballistic failure of rubber/metal laminates.

ACKNOWLEDGEMENTS

This work was supported by the Office of Naval Research, in part by Code 332 (R. G. Barsoum). TCR acknowledges an American Society for Engineering Education/Naval Research Laboratory postdoctoral fellowship.

REFERENCES

- ¹B. J. Russo and P. T. Savolainen, *Acc. Anal. Prev.* **117**, 216 (2018).
- ²A. Baroutaji, M. Sajjia, and A.-G. Olabi, *Thin-Walled Struct.* **118**, 137 (2017).
- ³H. Wu, S. Kuang, and H. Hou, *Int. J. Comp. Methods* **16**, 1950034 (2019).
- ⁴Z. Tao, Y. Jialin, Z. Xianglei, and Z. Bing, *Int. J. Comp. Methods* **16**, 1950042 (2019).
- ⁵D. Perna, M. A. Barucci, and M. Fulchignoni, *Astron. Astrophys. Rev.* **21**, 65 (2013).
- ⁶J. C. Ruiz-Suarez, *Rep. Prog. Phys.* **76**, 066601 (2013).
- ⁷Y. Qi and A. de Ruiter, *Icarus* **333**, 52 (2019).
- ⁸A. Kharazian and F. Lopez-Almansa, *Arch. Comp. Methods Eng.* **26**, 327 (2019).
- ⁹K. L. Hon, A. K. C. Leung, and A. R. Torres, *Semin. Pediatr. Neurol.* **30**, 117 (2019).
- ¹⁰D. A. Patton, *Appl. Bionics Biomech.* 7049743 (2016).
- ¹¹O. Duncan, T. Shepherd, C. Moroney, L. Foster, P. D. Venkatraman, K. Winwood, T. Allen, and A. Alderson, *Appl. Sci. (Basel)* **8**, 941 (2018).

- ¹²M. F. Sonnenschein, E. Nicoli, L. Ma, and B. L. Wendt, *Polymer* **131**, 25 (2017).
- ¹³A. Miranda-Vicario, P. M. Bravo, and F. Coghe, *Compos. Struct.* **203**, 233 (2018).
- ¹⁴C. A. Weisenbach, K. Logsdon, R. S. Salzar, V. C. Chancey, and F. Brozowski, *Mil. Med.* **183**, 287 (2018).
- ¹⁵X. Yang, *Lect. Notes Electr. Eng.* **527**, 433 (2019).
- ¹⁶A. Haris, H. P. Lee, and V. B. C. Tan, *Def. Technol.* **14**, 12 (2018).
- ¹⁷S. G. Kulkarni, X.-L. Gao, S. E. Horner, J. Q. Zheng, and N. V. David, *Compos. Struct.* **101**, 313 (2013).
- ¹⁸D. Marjoux, D. Baumgartner, C. Deck, and R. Willinger, *Acc. Anal. Prev.* **40**, 1135 (2008).
- ¹⁹D. Espíndola, S. Lee, and G. Pinton, *Phys. Rev. Appl.* **8**, 044024 (2017).
- ²⁰S. Rowson and S. M. Duma, *Ann. Biomed. Eng.* **39**, 2130 (2011); **41**, 873 (2013).
- ²¹M. L. Wilkins, *Int. J. Eng. Sci.* **16**, 793 (1978).
- ²²I. Levadnyi, J. Awrejcewicz, Y. Zhang, M. F. Goethel, and Y. Gu, *J. Med. Biol. Eng.* **38**, 587 (2018).
- ²³J. Sone, D. Kondziolka, J. H. Huang, and U. Samadani, *J. Neurosurg.* **126**, 768 (2017).
- ²⁴J. M. Varas, M. Philippens, S. R. Meijer, A. C. vandenBerg, P. C. Sibma, J. L. M. J. van Bree, and D. V. W. M. deVries, *Front. Neurol.* **2**, 58 (2011).
- ²⁵T. Rahimzadeh, E. M. Arruda, and M. D. Thouless, *J. Mech. Phys. Solids* **85**, 98 (2015).
- ²⁶J. A. O'Neill, C. A. Gunnarsson, P. Moy, K. A. Masser, J. L. Lenhart, and T. Weerasooriya, *Dyn. Behav. Mater.* **1**, 51 (2017).
- ²⁷R. B. Bogoslovov, C. M. Roland, and R. M. Gamache, *Appl. Phys. Lett.* **90**, 221910 (2007).
- ²⁸C. M. Roland, D. Fragiadakis, R. M. Gamache, and R. Casalini, *Philos. Mag.* **93**, 468 (2013).
- ²⁹R. A. Mrozek, B. Leighliter, C. S. Gold, Christopher, I. R. Beringer, J. H. Yu, M. R. VanLandingham, P. Moy, M. H. Foster, and J. L. Lenhart, *J. Mech. Behav. Biomed. Mater.* **44**, 109 (2015).
- ³⁰E. Antillon and A. Strachan, *J. Chem. Phys.* **142**, 084108 (2015).
- ³¹J. A. Pathak, J. N. Twigg, K. E. Nugent, D. L. Ho, E. K. Lin, P. H. Mott, C. G. Robertson, M. K. Vukmir, T. H. Epps, and C. M. Roland, *Macromolecules* **41**, 7543 (2008).
- ³²M. Grujicic, R. Yavari, J. S. Snipes, S. Ramaswami, J. Runt, J. Tarter, and G. Dillon, *J. Mater. Sci.* **47**, 8197 (2012).
- ³³Y.-C. M. Wu, W. G. Hu, Y. C. Sun, D. Veysset, S. E. Kooi, K. A. Nelson, T. M. Swager, and A. J. Hsieh, *Polymer* **168**, 218 (2019).
- ³⁴M. Grujicic, B. Pandurangan, T. He, B. A. Cheeseman, C.-F. Yen, and C. L. Randow, *Mater. Sci. Eng. A* **527**, 7741 (2010).
- ³⁵V. Agrawal, G. Arya, and J. Oswald, *Macromolecules* **47**, 3378 (2014).
- ³⁶M. V. Zhikharev and S. B. Sapozhnikov, *Int. J. Impact Eng.* **101**, 42 (2017).
- ³⁷H. W. Meyer and R. M. Brannon, *Int. J. Impact Eng.* **42**, 48 (2012).
- ³⁸D. A. Shockey, *Exp. Mech.* **47**, 581 (2007).
- ³⁹P. J. Hazell, M. R. Edwards, H. Longstaff, and J. Erskine, *Int. J. Impact Eng.* **36**, 147 (2009).
- ⁴⁰L. H. Nguyen, T. R. Laessig, S. Shannon, W. Riedel, A. P. Mouritz, and A. C. Orifici, *Compos. Part A Appl. Sci. Manuf.* **84**, 224 (2016).
- ⁴¹T. El Sayed, W. Mock, A. Mota, F. Fraternali, and M. Ortiz, *Comput. Mech.* **43**, 525 (2009).
- ⁴²Z. Xue and J. W. Hutchinson, *Int. J. Solids Struct.* **45**, 3769 (2008).
- ⁴³S. Futamura, *RUBBER CHEM. TECHNOL.* **64**, 57 (1991).
- ⁴⁴S. Futamura and A. A. Goldstein, *Tire Sci. Technol.* **32**, 56 (2004).
- ⁴⁵J. M. Gibert, B. Ananthasayanam, P. F. Joseph, T. B. Rhyne, and S. M. Cron, *Tire Sci. Technol.* **41**, 82 (2013).
- ⁴⁶W. V. Mars, *RUBBER CHEM. TECHNOL.* **84**, 178 (2011).
- ⁴⁷R. G. Barsoum, *Elastomeric Polymers with High Rate Sensitivity: Applications in Blast, Shockwave, and Penetration Mechanics*, Elsevier, Norwich, NY, 2015.
- ⁴⁸M. R. Amini and S. Nemat-Nasser, *Int. J. Fract.* **162**, 205 (2010).
- ⁴⁹L. Xue, W. Mock, and T. Belytschko, *Mech. Mater.* **42**, 981 (2010).

- ⁵⁰C. M. Roland, D. Fragiadakis, and R. M. Gamache, *Compos. Struct.* **92**, 1059 (2010).
- ⁵¹Z. Jia, Y. Yu, and L. Wang, *Mater. Des.* **168**, 107650 (2019).
- ⁵²X. Xuan, Y.-R. Miao, W. L. Shaw, K. S. Suslick, and D. D. Dlott, *J. Am. Chem. Soc.* **141**, 2220 (2019).
- ⁵³S. K. Yeh, J. J. Lin, H. Y. Zhuang, Y. C. Chen, H. C. Chang, J. Y. Zheng, L. Y. Yang, K. C. Lee, Y. L. Chen, and S. P. Rwei, *J. Polym. Res.* **26**, 155 (2019).
- ⁵⁴L. D. Pye and M. Affatigato, Eds., Special Issue: Glass Armor and General Glass Science. *Int. J. Appl Glass Sci.* **5**, (2015).
- ⁵⁵G. Montella, C. B. Giller, A. P. Holt, D. Fragiadakis, R. M. Gamache, and C. M. Roland, *J. DoD Res. Eng.*, in press (2020).
- ⁵⁶C. M. Roland, *Viscoelastic Behavior of Rubbery Materials*, Oxford University Press, New York, 2011.
- ⁵⁷C. M. Roland and R. M. Gamache, Measuring the Blast and Ballistic Performance of Armor, NRL Formal Report, NRL/FR/6126-15-10, 284, Naval Research Laboratory, Washington, D.C. (2015).
- ⁵⁸L. J. Briggs, *J. Res. Natl. Bur. Stand.* **34**, 1 (1945).
- ⁵⁹W. G. Knauss, *Int. J. Fract.* **196**, 99 (2015).
- ⁶⁰C. M. Roland, RUBBER CHEM. TECHNOL. **79**, 429 (2006).
- ⁶¹P. G. Santangelo and C. M. Roland, RUBBER CHEM. TECHNOL. **65**, 965 (1992).
- ⁶²P. H. Mott, J. N. Twigg, C. M. Roland, K. E. Nugent, T. E. Hogan, and C. G. Robertson, *J. Polym. Sci. Polym. Phys. Ed.* **49**, 1194 (2011).

[Received October 2019, Revised January 2020]